J. Vis. Commun. Image R. 21 (2010) 343–354

Contents lists available at ScienceDirect

J. Vis. Commun. Image R.

journal homepage: www.elsevier.com/locate/jvci

Integrating local distribution information with level set for boundary extraction

Lei He [a,*], Songfeng Zheng [b], Li Wang [c]

[a] Department of Information, Computing, and Engineering, College of Science and Technology, Armstrong Atlantic State University, 11935 Abercorn Street, Savannah, GA 31419, USA
[b] Department of Mathematics, Missouri State University, Springfield, MO 65897, USA
[c] School of Computer Science and Technology, Nanjing University of Science and Technology, Nanjing 210094, PR China

ARTICLE INFO

Article history:
Received 18 May 2009
Accepted 13 February 2010
Available online 1 March 2010

Keywords:
Image segmentation
Implicit active contour
Gaussian mixture model
Hueckel edge operator
Zernike moments
Local distribution fitting
Level set without initial contour
Piecewise smooth image

ABSTRACT

This paper presents a general object boundary extraction model for piecewise smooth images, which incorporates local intensity distribution information into an edge-based implicit active contour. Unlike traditional edge-based active contours that use gradient to detect edges, our model derives the neighborhood distribution and edge information with two different region-based operators: a Gaussian mixture model (GMM)-based intensity distribution estimator and the Hueckel operator. We propose the local distribution fitting model for more accurate segmentation, which incorporates the operator outcomes into the recent local binary fitting (LBF) model. The GMM and the Hueckel model parameters are estimated before contour evolution, which enables the use of the proposed model without the need for initial contour selection, i.e., the level set function is initialized with a random constant instead of a distance map. Thus our model essentially alleviates the initialization sensitivity problem of most active contours. Experiments on synthetic and real images show the improved performance of our approach over the LBF model.

1. Introduction

Image segmentation is a fundamental task in image processing and computer vision, which has been studied extensively in past decades. Most existing segmentation methods can be roughly categorized, based on the image features used, into two basic approaches, the edge-based and region-based methods [7]. Typical difficulties in image segmentation include noise, low intensity contrast with weak edges, and intensity inhomogeneity [16], which pose significant challenges to traditional segmentation methods like region growing and edge detection [17]. In addition, traditional edge detection approaches like thresholding need further edge linking operation to produce continuous object boundaries. To address these difficulties, more recent methods, such as the active contour models, including the key concepts of both the edge-based [23,6,20] and region-based approaches [9,19,34-36,39], have been proposed for image segmentation with promising results. The active contour models can achieve subpixel accuracy and provide closed and smooth contours/surfaces. See [16,11] for a review of major active contour models.

Edge-based active contour models [23,6,20] generally use image gradient for object boundary detection, which are usually sensitive to noise and weak edges. To solve such problems, region information (e.g. intensity, color and texture descriptors) has been used in active contours [9,19,34-36,39], which usually segment an image into multiple regions of interest with certain homogeneity constraints. In addition, region-based active contours are much less sensitive to contour initialization than edge-based models.

In practice, implicit active contour models (level set methods) are commonly used in situations where contour topology changes in deformation, which cannot be simply handled by explicit active contours (snakes). A major category of region-based level set methods is proposed to minimize the well-known Mumford and Shah (MS) functional [27]. Due to the difficulty of directly minimizing the MS functional, different approximation methods [1,2,34,9,35,30,15] have been proposed to allow more efficient energy minimization. For example, early phase field models [1,2] use elliptic approximations by Γ–convergence to the weak formulation of the MS functional. A recent paper [30] presents a new primal-dual algorithm to minimize a convex relaxation of the MS functional, which is independent of initialization. For image segmentation, the piecewise constant (PC) models [36,9] approximate an image as a combination of a set of homogenous regions, which is not true for images with intensity inhomogeneity. For example, the Chan–Vese (CV) model [9] assumes homogeneous object and background regions with distinct intensity means. In [34,35], more advanced piecewise smooth (PS) models have been proposed to improve the PC model performance in case of intensity inhomogeneity. However, with rather complicated algorithms, these models are usually computationally expensive. For more efficient and robust segmentation, a recent Graph Cuts-based method [15] is proposed

* Corresponding author. Fax: +1 912344 3491.
E-mail address: Lei.He@armstrong.edu (L. He).

1047-3203/$ - see front matter © 2010 Elsevier Inc. All rights reserved.
doi:10.1016/j.jvcir.2010.02.009

to reformulate the Mumford–Shah functional on an arbitrary graph, which is optimized by combinatorial techniques. As indicated in [18], the models using global image statistics usually have difficulty to extract heterogeneous objects. To overcome this problem, recently localized region-based models [5,29,26,19,18,32] have been proposed. For example, in [19], a local binary fitting (LBF) energy is defined over the neighborhood of each image pixel, and the active contour is deformed to minimize the integration of the LBF energy through the whole image. In each neighborhood, the intensity means (f_1 and f_2) of background and objects are estimated and used in the energy to fit the local intensity distribution. With the simple estimation of f_1 and f_2, this model has difficulty in some complex segmentation problems, e.g. multiple objects with complex shapes. In addition, like most existing active contours, the LBF model is rather sensitive to the initial contour location. Last but not least, the values of f_1 and f_2 have to be estimated in each contour evolution, which introduces expensive computational cost.

Other similar localized energy functional can be seen in [5,29,26,18,32]. Brox and Cremers [5] extends the work of Zhu and Yuille [39] to further study the relationship between the full piecewise smooth Mumford–Shah functional and Bayesian model. According to the linear filtering operation of a regularization framework, it is shown that the MS functional can be interpreted as a first-order approximation of a Bayesian a-posteriori maximization based on local intensity statistics, i.e., a Gaussian distribution with fixed variance. Furthermore, they extend the traditional MS functional by incorporating the variable local variance for a more robust segmentation. Similarly, Piovano et al. [29] replace the global region intensity mean in the piecewise constant MS functional (i.e., the CV PC model [9]) with a piecewise smooth function that corresponds to the intensity average in a small neighborhood of an image point. This new model approximates the original piecewise smooth MS functional, but with a simpler complexity similar to the CV PC model. Though, like the LBF model, the local intensity means and two boundary terms have to be updated in each level set evolution, which still demands a high computational cost. In [26], Mory et al. propose a fuzzy region competition model to partition an image into foreground and background regions, which employs a fuzzy membership function instead of using active contours for segmentation. Based on the original region competition algorithm [39], a general non-parametric region error function is used for intensity density estimation in the foreground and background regions. The foreground region in [39] is replaced by the fuzzy membership function, which enables a model more computational efficient and less sensitive to initialization than active contour models. Moreover, the model is extended for more general case of local space-varying probability densities, with the same energy functional as the LBF model. In [32], a two-step algorithm combining the global CV PC energy and a new local energy is proposed for angiograms vessel segmentation. The CV model is applied in the first step to roughly extract the vessels and the local energy term is used in the second step to refine the result, which is constructed similar to the CV term but based on the intensity contrast within the level set narrowband. In [18], a general framework is proposed to reformulate current global region-based energy to a local form. Three global energy functions have been used as examples to show the improved performance when adapted into the framework. Specifically, the uniform modeling energy is similar to the LBF energy since both of them are based on the CV PC model [9]. Same as the approaches in [19,29], the model in [18] has a high computational cost by updating the local statistics in each iteration. In addition, these active contour-based local models are usually sensitive to contour initialization, see Section 4, where we compare our proposed method with the LBF model and the local region-based approach in [18] with different energies.

Based on the LBF model, we present a new edge-based active contour that uses a more general and accurate local region model, *local distribution fitting* (LDF) energy, to characterize the neighborhood intensity distribution for edge detection in piecewise smooth (non-textured) images. Unlike traditional edge-based active contours that use image gradient for edge detection, two localized region-based operators, a Gaussian mixture model (GMM) [25]-based intensity distribution estimator and the Hueckel operator [17], are used to obtain neighborhood distribution and edge information before contour evolution. The pre-derived neighborhood distribution depends only on the image itself, which is used in the LDF model for object boundary extraction. This enables an implicit active contour without the initial contour selection, i.e., the level set function can be initialized as a random constant instead of a distance map. For the local GMM-based distribution estimator, the neighbor intensities of each image point are characterized by a mixture of two Gaussian distributions of object and background. The GMM parameters are estimated by the expectation–maximization (EM) [12] algorithm. We further improve the algorithm efficiency by using another neighborhood-based operator, the Hueckel operator, to derive the edge parameters of each region, which are computed by a set of orthogonal Zernike moments [22]. We present these two operators as examples of how traditional edge detection approaches can be incorporated into current active contours, and make no claim that one operator outperforms the other. The LDF energy terms for all image points are integrated together as the level set energy functional, based on which the contour evolution equation is derived. Compared to the LBF model and other existing approaches (e.g. PC and PS models), there are three major contributions of the proposed LDF model: (a) a general object boundary extraction model is proposed for more accurate and robust segmentation, which incorporates different region-based operator outcomes of neighborhood distribution information into an implicit active contour; (b) the initialization sensitivity problem is essentially alleviated with a "random" level set initialization; and (c) the moment-based LDF model saves computational cost.

The remainder of this paper is organized as follows. Section 2 reviews the background of two well-known region-based active contour methods (Mumford–Shah and Chan–Vese models), GMM and EM, and the Hueckel operator and Zernike moments. Section 3 presents the proposed LDF model. Experimental results on a set of synthetic and in vivo images are illustrated in Section 4. This paper is summarized in Section 5.

2. Background

2.1. Mumford–Shah model

Given a gray scale image I: $\Omega \subset \Re^2 \to \Re$ Mumford and Shah [27] formulated image segmentation as a problem of finding an optimal contour C that divides Ω into a set of regions Ω_i, and a piecewise smooth approximation u of I, which is smooth in each region Ω_i, i.e., a denoised version of I. The energy functional was defined as:

$$E(u,C) = \int_{\Omega} (u-I)^2 d\mathbf{x} + \mu \int_{\Omega\setminus C} |\nabla u|^2 d\mathbf{x} + \nu |C|, \tag{1}$$

where $\mathbf{x} \in \Re^2$, $|C|$ is the contour length, $\mu > 0$ and $\nu > 0$ are constants to balance the terms. The first term is the data fidelity term; the second term is a regularization term; and the third term is the contour length term. In practice, it is difficult to solve Eq. (1) directly due to different dimensions of u and C, and the non-convexity of the energy functional. Based on Eq. (1), many simplified models have been proposed for practical applications, e.g. elliptic approximations

[1,2], CV PC model [9], PS models [34,35], and Graph Cuts-based model [15].

2.2. Chan–Vese piecewise constant model

Chan and Vese [9] proposed the well-known PC model to overcome the classical snakes' problems of sensitivity to image noise and initial contour location, which is defined as:

$$E(c_1,c_2,C)=\int_{out(C)}(I-c_1)^2d\mathbf{x}+\int_{in(C)}(I-c_2)^2d\mathbf{x}+\nu|C|, \tag{2}$$

where $out(C)$ and $in(C)$ are the regions outside and inside the active contour C, respectively, and c_1 and c_2 are two global constants representing the intensity means of the two regions, i.e., background and objects. Eq. (2) can be reformulated in level set framework as:

$$E(c_1,c_2,\phi)=\int_\Omega(I_0-c_1)^2H(\phi)d\mathbf{x}+\int_\Omega(I_0-c_2)^2(1-H(\phi))d\mathbf{x}+\nu\int_\Omega|\nabla H(\phi)|d\mathbf{x}, \tag{3}$$

where H is the Heaviside step function and φ represents the level set function. By calculus of variations, the level set evolution equation can be derived as:

$$\frac{\partial\phi}{\partial t}=\delta_\varepsilon(\phi)\left[div\left(\frac{\nabla\phi}{|\nabla\phi|}\right)-(I_0-c_1)^2+(I_0-c_2)^2\right], \tag{4}$$

where $c_1(\phi)=\frac{\int_\Omega I_0H_\varepsilon d\mathbf{x}}{\int_\Omega H_\varepsilon d\mathbf{x}}$, $c_2(\phi)=\frac{\int_\Omega I_0(1-H_\varepsilon)d\mathbf{x}}{\int_\Omega(1-H_\varepsilon)d\mathbf{x}}$. H_ε is a modified Heaviside function for a smooth Dirac function: $H_\varepsilon(x)=\frac{1}{2}[1+\frac{2}{\pi}\arctan(\frac{x}{\varepsilon})]$, $\delta_\varepsilon(x)=H'_\varepsilon(x)=\frac{1}{\pi}\frac{\varepsilon}{\varepsilon^2+x^2}$.

The constants c_1 and c_2 in the CV PC model cannot accurately characterize inhomogeneous regions in real data, which results in incorrect segmentation for images with intensity inhomogeneity. To address this problem, Vese and Chan developed the PS model [35], which is computationally expensive. As indicated in [18], recent localized active contours [5,29,19,18,32] are all based on the CV PC model.

2.3. GMM and the EM algorithm

Mixture models [25] are widely used to approximate complicated distributions with the output coming from one of a group of "hidden" sources (e.g. objects and background in an image). In statistics, a mixture model is usually defined as a probability distribution that is a convex combination of several independent components with different probability distributions. Therefore, it provides a general framework to characterize heterogeneity. Given an output of a mixture model, the goal is to estimate from which source (measured by probabilities) the output is generated, as well as the parameters describing the source component distributions, e.g. means and variances of a Gaussian mixture model. As a popular model, GMM has been widely used in image segmentation applications [3,28,31] to characterize the objects and background intensity distributions.

Given a set of N samples (e.g. image points) from n-dimensional space, $X=\{\mathbf{x}_1,\ldots,\mathbf{x}_j,\ldots,\mathbf{x}_N\}$, in which each sample is drawn from one of M Gaussian components, a GMM can be denoted as:

$$p(X|\Theta)=\sum_{i=1}^{M}\alpha_ip_i(X|\theta_i), \tag{5}$$

where the parameters are $\Theta=\{\alpha_1,\ldots,\alpha_M,\theta_1,\ldots,\theta_M\}$ such that $\sum_{i=1}^{M}\alpha_i=1$ and α_i refers to the prior probability of each component; $\theta_i=(\mu_i,\Sigma_i)$, μ_i is the mean and $\sum_i$ is the covariance matrix,

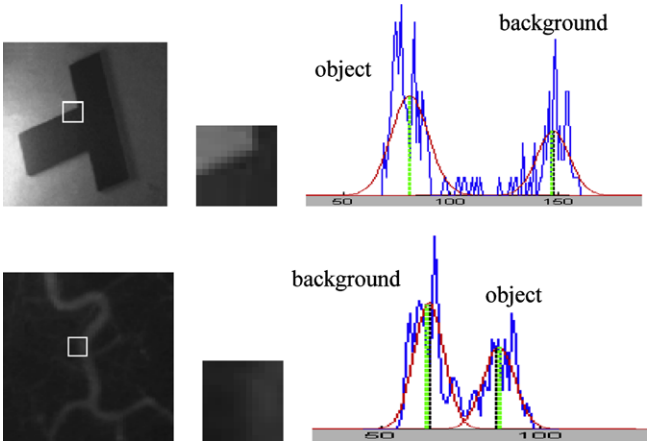

Fig. 1. Local GMM distribution estimation examples.

$i=1,\ldots M$. Let y_j, $j=1,\ldots N$, denote which Gaussian $\mathbf{x}_j$ is drawn from, the probability of $\mathbf{x}_j$ coming from the i-th Gaussian is:

$$P(\mathbf{x}_j|y_j=i,\theta_i)=\frac{1}{(2\pi)^{n/2}|\Sigma_i|^{1/2}}\exp\left(-\frac{1}{2}(\mathbf{x}_j-\mu_i)^T\Sigma_i^{-1}(\mathbf{x}_j-\mu_i)\right), \tag{6}$$

The task is to estimate the hidden distributions given the data, i.e., to estimate the unknown parameters θ which maximize Eq. (5). The GMM parameters can be estimated by the EM algorithm [12], which repeats the E-step and M-step until convergence. The E-step is to calculate the expectation of which Gaussian is used, conditioned on the observations (X), using the estimated prior probability of each distribution ($p(y_j=i|\theta_i)$) and current parameter values (Θ_t),

$$p(y_j=i|\mathbf{x}_j,\Theta_t)=\frac{p(\mathbf{x}_j|y_j=i,\Theta_t)p(y_j=i|\Theta_t)}{\sum_{k=1}^{M}p(\mathbf{x}_j|y_j=k,\Theta_t)p(y_j=k|\Theta_t)}. \tag{7}$$

Given the E-step estimation of unknown variables ($\mathbf{y}=\{y_1,\ldots,y_N\}$, $y_j=1,\ldots,M$), the M-step estimates the distribution parameters (Θ) and the prior probability of each distribution, which maximize the data likelihood as

$$Q(\Theta,\Theta_t)=E_y\left[\log\prod_{j=1}^{N}p(\mathbf{x}_j,\mathbf{y}|\Theta)|\mathbf{x}_j\right]=\sum_{j=1}^{N}\sum_{i=1}^{M}p(y_j=i|\mathbf{x}_j,\Theta_t)\log(p(\mathbf{x}_j|y_j=i,\Theta)p(y_j=i|\Theta)), \tag{8}$$

where the log-likelihood is used for easier numerical implementation. With gradient ascent approach, we can update the parameters and the prior probabilities as:

$$\mu_i=\frac{\sum_{j=1}^{N}p(y_j=i|\mathbf{x}_j,\Theta_t)\mathbf{x}_j}{\sum_{j=1}^{N}p(y_j=i|\mathbf{x}_j,\Theta_t)},\quad \Sigma_i=\frac{\sum_{j=1}^{N}p(y_j=i|\mathbf{x}_j,\Theta_t)(\mathbf{x}_j-\mu_i)(\mathbf{x}_j-\mu_i)^T}{\sum_{j=1}^{N}p(y_j=i|\mathbf{x}_j,\Theta_t)},\quad \alpha_i=p(y_j=i|\Theta_t)=\frac{1}{N}\sum_{j=1}^{N}p(y_j=i|\mathbf{x}_j,\Theta_t) \tag{9}$$

These updated parameters then become the input for next E-step, and the convergence to a local maximum of the EM algorithm is guaranteed [12,38]. In our application, only the distributions of objects and background exist in a small neighborhood, i.e., $M=2$. Using the EM algorithm, Fig. 1 shows two examples of local GMM-based distribution estimation in a small region (see the

white rectangles). The left images in Fig. 1 are input images with intensity inhomogeneity, and the middle images are the enlarged views of the selected regions. The blue curves in the right images are the intensity histograms of the regions. The estimated Gaussian distributions of the objects and background are illustrated as the red curves, with the black dotted lines as the estimated intensity means using Eq. (9). It can be seen that the estimated means match well with the real intensity means (green lines), which show the suitability to use the localized GMM for neighborhood distribution estimation. In the proposed LDF model, we use GMM to estimate the local intensity means f_1 and f_2 of the LBF model, which is more accurate than the LBF model.

2.4. Hueckel operator and Zernike moments

The Hueckel operator [17] models an edge as a step discontinuity intensity at a location in an image. As shown in Fig. 2, a step function is modeled in a unit circle as:

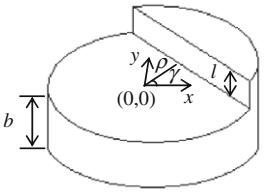

$$f(x,y)=\begin{cases} b & ;\ \text{if } (x\cos\gamma+y\sin\gamma)<\rho \\ b+l & ;\ \text{if } (x\cos\gamma+y\sin\gamma)>\rho \end{cases}$$

Fig. 2. Hueckel operator model.

where l is the step height, b is the base intensity, ρ and γ define the position and orientation of the edge segment with respect to the center of the circle. Thus the two intensities b and $(b+l)$ correspond to the intensity means of object and background in the region.

In the proposed model, a set of image moments, Zernike moments [22], are used to estimate these four parameters of b, l, ρ, and γ. Zernike moments are projections of the image data onto a set of complex polynomials, which form a complete orthogonal set over the interior of a unit circle. To evaluate the Zernike moments at a pixel, the neighborhood of that pixel should be mapped to the interior of the unit circle. The Zernike moment of order n and repetition m is defined as

$$A_{nm}=\frac{n+1}{\pi}\sum_x\sum_y I(x,y)V^*_{nm}(r,\omega), \tag{10}$$

where $V_{nm}(r,\omega)$ is a complex polynomial and defined as

$$V_{nm}(r,\omega)=R_{nm}(r)e^{jm\omega}, \tag{11}$$

with $j=\sqrt{-1}$, $n\geqslant 0$, and $n-|m|$ is an even positive integer and $R_{nm}(r)$ is a radial polynomial defined as

$$R_{nm}(r)=\sum_{s=0}^{(n-|m|)/2}\frac{(-1)^s(n-s)!r^{n-2s}}{s!\left(\frac{n+|m|}{2}-s\right)!\left(\frac{n-|m|}{2}-s\right)!}, \tag{12}$$

In Eq. (10), V^*_{nm} is the conjugate of V_{nm}. As in [22], we can compute the parameters as:

$$\gamma=\tan^{-1}\left(\frac{\mathrm{Im}[A_{11}]}{\mathrm{Re}[A_{11}]}\right),\quad \rho=\frac{A_{20}}{A'_{11}},\quad l=\frac{3A'_{11}}{2(1-\rho^2)^{3/2}},$$

$$b=\frac{A_{00}-\frac{l\pi}{2}+l\sin^{-1}(\rho)+l\rho\sqrt{(1-\rho^2)}}{\pi},\ \text{where } A'_{11}=A_{11}e^{j\gamma}. \tag{13}$$

Different from the local GMM-based distribution estimation, here the edge parameters are computed directly by Eq. (13) instead of the iterative EM algorithm, which saves the algorithm computational cost. Similar to Fig. 1, the estimated b and $b+l$ are close to the real intensity means.

3. Proposed approach

3.1. Local distribution fitting energy functional

In order to improve the performance of the global PC [9] and PS [34,35] models on images with inhomogeneity, Li et al. [19] proposed the implicit active contours driven by the LBF energy. The level set energy function of the LBF model is defined as

$$E(\phi,f_1,f_2)=E^{LBF}(\phi,f_1,f_2)+\mu P(\phi)+\nu L(\phi), \tag{14}$$

where $E^{LBF}(\varphi,f_1,f_2)$ is the LBF energy, $P(\varphi)$ is a level set regularization term [20,21] which penalizes the deviation of the level set function from a signed distance function, $L(\varphi)$ is the contour length term which prefers a smooth curve.

In the LBF energy functional, two local intensity fitting functions, $f_1(\mathbf{x})$ and $f_2(\mathbf{x})$, $\mathbf{x}\in\Re^2$, are used to approximate the intensity means of the two local regions around the point $\mathbf{x}$ outside and inside the active contour, i.e., the background and object regions. The LBF energy functional is constructed as:

$$\begin{aligned}E^{\mathrm{LBF}}(\phi,f_1,f_2)=&\lambda_1\int\left[\int K_\sigma(\mathbf{x}-\mathbf{y})|I(\mathbf{y})-f_1(\mathbf{x})|^2H(\phi(\mathbf{y}))d\mathbf{y}\right]d\mathbf{x}\\&+\lambda_2\int\left[\int K_\sigma(\mathbf{x}-\mathbf{y})|I(\mathbf{y})-f_2(\mathbf{x})|^2(1-H(\phi(\mathbf{y})))d\mathbf{y}\right]d\mathbf{x},\end{aligned} \tag{15}$$

where $\lambda_1>0$ and $\lambda_2>0$ are constants, $K_\sigma(\mathbf{x}-\mathbf{y})$ is the Gaussian kernel function as

$$K_\sigma(d)=\frac{1}{\sqrt{2\pi}\sigma}e^{-|d|^2/2\sigma^2},\ \text{with a scale parameter } \sigma>0.$$

This local Gaussian kernel restricts the LBF energy of each point in a small neighborhood. The regularizing term $P(\varphi)$ [20,21][1] intrinsically maintains the regularity of the level set function without the need for extra re-initialization procedures, which is defined as

$$P(\phi)=\int_\Omega\frac{1}{2}(|\nabla\phi(\mathbf{x})|-1)^2d\mathbf{x}. \tag{16}$$

The contour length term $L(\varphi)$ is defined as

$$L(\phi)=\int_\Omega\delta(\phi(\mathbf{x}))|\nabla\phi(\mathbf{x})|d\mathbf{x}, \tag{17}$$

where $\delta(\varphi)$ is the Dirac delta function. The local fitting functions $f_1(\mathbf{x})$ and $f_2(\mathbf{x})$ are computed as:

$$f_1(\mathbf{x})=\frac{K_\sigma(\mathbf{x})*[H(\phi(\mathbf{x}))I(\mathbf{x})]}{K_\sigma(\mathbf{x})*H(\phi(\mathbf{x}))},\quad \text{and}$$
$$f_2(\mathbf{x})=\frac{K_\sigma(\mathbf{x})*[(1-H(\phi(\mathbf{x})))I(\mathbf{x})]}{K_\sigma(\mathbf{x})*[1-H(\phi(\mathbf{x}))]}, \tag{18}$$

which depend on the level set function φ and need to be updated in each contour evolution.

The LBF model improves the global PC and PS models on intensity inhomogeneity and is more computationally efficient than the PS models. Nevertheless, with only two simply estimated intensity means for local regions, this model has problems in complex image segmentation, e.g. multiple objects with complex shapes (see Section 4). Moreover, the LBF model is rather sensitive to the initial contour location, as will be shown in our experiments. Last but not least, the updating of the $f_1(\mathbf{x})$ and $f_2(\mathbf{x})$ in each iteration still demands a high computational cost. To overcome these problems,

[1] Note there are also other methods [14,37] proposed to eliminate the need for reinitializing the level set function during evolution process, which is usually implemented efficiently by the first order approximation [33].

especially for a robust contour initialization, we propose the LDF energy for each point $\mathbf{x}$ as:

$$E_{\mathbf{x}}^{\mathrm{LDF}}(\phi) = \lambda_1 \int K_\sigma(\mathbf{x}-\mathbf{y})|I(\mathbf{y}) - h_1(\mathbf{x})|^2 H(\phi(\mathbf{y}))d\mathbf{y} + \lambda_2 \times \int K_\sigma(\mathbf{x}-\mathbf{y})|I(\mathbf{y}) - h_2(\mathbf{x})|^2 (1 - H(\phi(\mathbf{y})))d\mathbf{y}, \quad (19)$$

where $h_1(\mathbf{x})$ and $h_2(\mathbf{x})$ correspond to the local background and object distribution fitting functions, respectively. Using Eq. (9) or Eq. (13), h_1 and h_2 can be obtained by the local GMM-based operator or the Hueckel operator before contour evolution. With localized GMM, two Gaussian distributions of object and background are mixed in the small neighborhood of each image point. The estimated intensity means (μ_1 and μ_2 in Eq. (9)) correspond to h_1 and h_2. For the Hueckel edge model, we compute b and $(b + l)$ (Eq. (13)) as h_1 and h_2.

Before contour evolution, we determine the correspondence of the pre-calculated μ_1, μ_2 (or b, $b + l$) to h_1, h_2 according to the relative brightness of background and objects, which can be simply obtained as prior knowledge of an input image. For example, if objects are always locally (in a small neighborhood) darker than the background, we have $h_1 = \max(\mu_1, \mu_2)$ (or $b + l$) and $h_2 = \min(\mu_1, \mu_2)$ (or b). Thus h_1 and h_2 depend on the image itself instead of the level set function, which can be computed offline with a more efficient computational cost than the LBF model. In addition, the pre-derived h_1 and h_2 essentially enables an active contour model without user initialization, i.e., the level set function can be initialized with a random constant, see Section 3.3. Therefore the LDF model essentially alleviates the initialization sensitivity problem of the LBF model and many existing active contours. Note that the recent algorithm [30] that minimizes a convex relaxation of the MS functional does not assume any image priors, which is independent of initialization and may be applied for segmentation applications to overcome the initialization sensitivity problem.

For object boundary detection, we integrate the LDF energy at each point over the whole image. Together with the level set regularizing term $P(\varphi)$ of Eq. (16) and the contour length term $L(\varphi)$ of Eq. (17), we construct the level set energy similar to Eq. (14):

$$E(\phi, h_1, h_2) = E^{\mathrm{LDF}}(\phi, h_1, h_2) + \mu P(\phi) + \nu L(\phi) = \int_\Omega E_{\mathbf{x}}^{\mathrm{LDF}}(\phi) + \frac{\mu}{2}(|\nabla\phi(\mathbf{x})| - 1)^2 + \nu\delta(\phi(\mathbf{x}))|\nabla\phi(\mathbf{x})|d\mathbf{x}. \quad (20)$$

Following [9,35,19], we use the modified Heaviside function for a smooth Dirac function (Eq. (4)), with $\varepsilon = 1$ in experiments.

3.2. Energy minimization

Gradient decent method is used to minimize the energy functional of Eq. (20). The level set evolution equation is:

$$\frac{\partial\phi}{\partial t} = -\delta_\varepsilon(\phi)(\lambda_1 e_1 - \lambda_2 e_2) + \mu\left[\nabla^2\phi - div\left(\frac{\nabla\phi}{|\nabla\phi|}\right)\right] + \nu\delta_\varepsilon(\phi)div\left(\frac{\nabla\phi}{|\nabla\phi|}\right), \quad (21)$$

where $e_1(\mathbf{x})$ and $e_2(\mathbf{x})$ are functions as $e_k(\mathbf{x}) = \int K_\sigma(y - x)|I(\mathbf{x}) - h_k(\mathbf{y})|^2 d\mathbf{y}$, $k = 1, 2$. For a point $\mathbf{x}$ far away from boundaries, the local intensity distributions of $h_1(\mathbf{x})$ and $h_2(\mathbf{x})$ are close to each other, thus the edge detection term $(\lambda_1 e_1 - \lambda_2 e_2)$ is small and the contour length term (the third term in Eq. (21)) dominates, which prevents the emergence of contours in these regions. On the other hand, for points located at edges, the term $(\lambda_1 e_1 - \lambda_2 e_2)$ is large due to the large difference of h_1 and h_2, thus it takes effect to detect boundaries.

3.3. Remarks on the LDF contour initialization

The level set function of the proposed LDF model is initialized with any constant (e.g. $\varphi = 1$). As described in Section 3.2, before contour evolution, we assign the pre-calculated neighborhood-based distribution parameters (μ_1 and μ_2, or b and $b + l$) to the LDF functions of h_1 (background) and h_2 (objects). In the level set evolution equation (Eq. (21)), $(\lambda_1 e_1 - \lambda_2 e_2)$ is small for points far away from boundaries and the contour length term dominates, resulting in fast convergence in these regions. Here we use the points near boundaries to show the emergence of zero level sets from the initial constant φ. For these points, the first term $(\lambda_1 e_1 - \lambda_2 e_2)$ dominates due to the large difference of the h_1 and h_2. Without loss of generality, we assume an image with objects locally brighter than background (e.g. Fig. 3(a)), i.e., $h_1 < h_2$. With $\lambda_1 = \lambda_2$, $(\lambda_1 e_1 - \lambda_2 e_2) > 0$ for the object points close to boundaries. Thus the φ values of these points decrease as the contour evolves with Eq. (21). Meanwhile, the φ values of the background points near boundaries increase with $(\lambda_1 e_1 - \lambda_2 e_2) < 0$. New contours (zero level sets) emerge as the φ values of object points finally become negative. Similar process can be obtained for objects locally darker than background. Therefore, with the pre-derived LDF functions of h_1 and h_2, we can initialize the level set function with any constant, which has also been shown in the experiments (e.g. Figs. 3, 7(b–c)).

4. Experiments

This section presents the experiments on both synthetic and real images with intensity inhomogeneity, noise and complex object shapes. Specifically, we compare our LDF model to the LBF model [19] and the local region-based approach (LR)[2] [18] on initialization sensitivity and segmentation accuracy. We also present several CV PC [9] and PS [35] model examples to show the limitations of the models using global statistics. For the experiments, the initial contours of the PC, PS, LBF, and LR models are shown in green and the red curves are segmentation results. For all these experiments, the level set function is initialized with a constant between 0 and 1 for the LDF model. The neighborhood size of 11 by 11 is used to estimate the local GMM and Hueckel operator parameters (i.e., the unit circle). Note that the GMM and Hueckel operators are two different examples to estimate the LDF functions. Similar to the three energy examples presented in [18], we do not suggest that one is superior to the other according to accuracy and robustness. A common feature of these images is that the objects are always locally (i.e., within a small region) brighter (Fig. 3(a)) or darker (Fig. 4(a)) than the background, which may not be true in the whole images. According to this feature, after the derivation of μ_1 and μ_2 (or b and l) of each image point, we can determine their correspondence to h_1 and h_2, as described in Section 3.2.

Figs. 3(a) and 4(a) are two images from [19] with intensity inhomogeneity. They share the common feature as described above. For example, although the object in Fig. 3(a) is always locally brighter than the background, the left part of object is darker than the right background. The active contours using global statistics usually have difficulty to handle such intensity inhomogeneity problem, e.g. the CV PC model results in Figs. 3(b–c) and 4(b–c), and the PS model result in Fig. 4(e). It can be seen that the PS model outperforms the PC model on intensity inhomogeneity, as shown in Fig. 3(d–e) and Fig. 4(d). Though, the CV PC model is rather insensitive to the contour initialization, i.e., it produces almost the same

[2] The uniform modeling (UM) energy and the mean separation (MS) energy in [18] are compared in the experiments, and the histogram separation (HS) energy is not included in the comparison due to its very high computational and time cost.

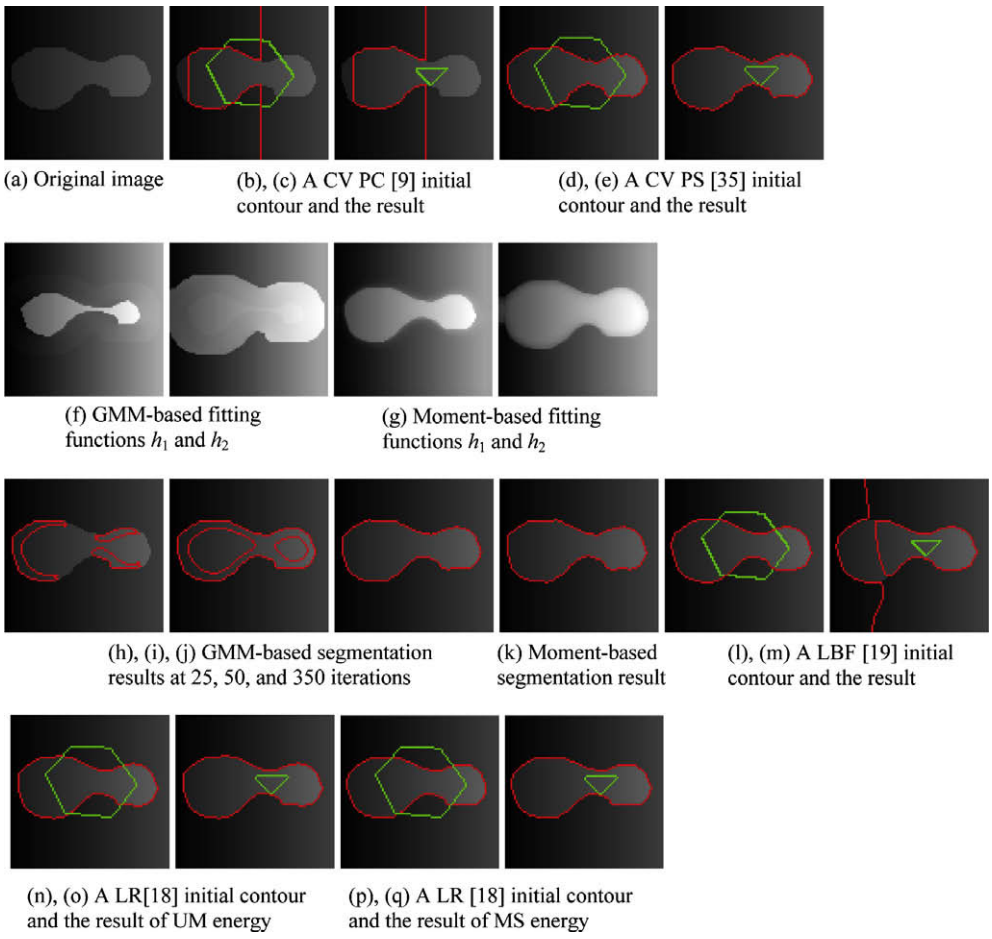

Fig. 3. An example with synthetic intensity inhomogeneity.

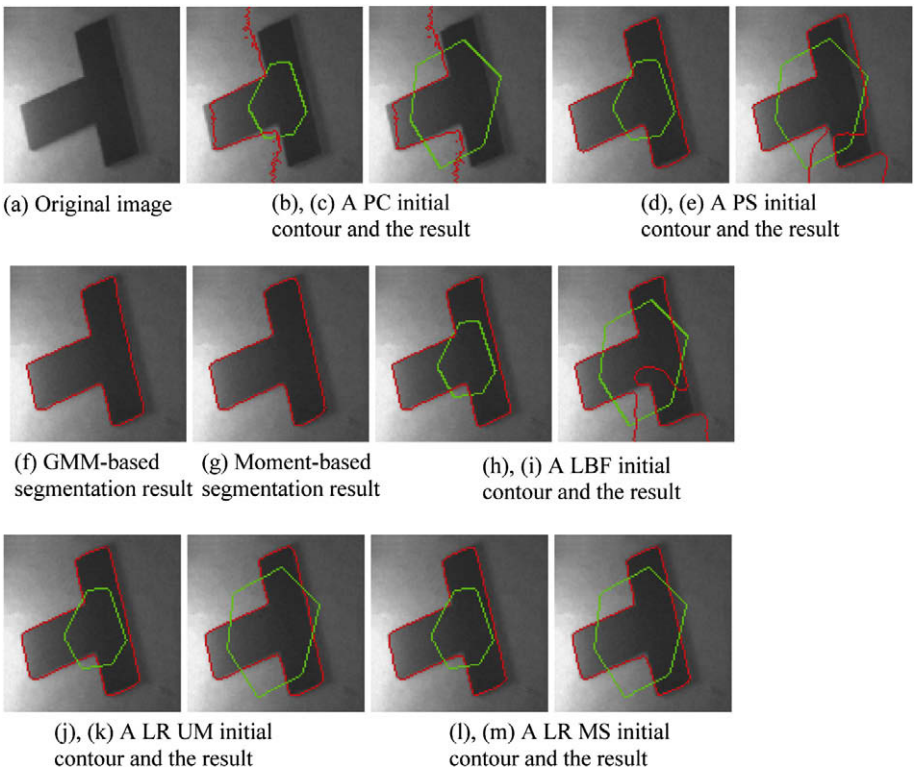

Fig. 4. A real image with intensity inhomogeneity.

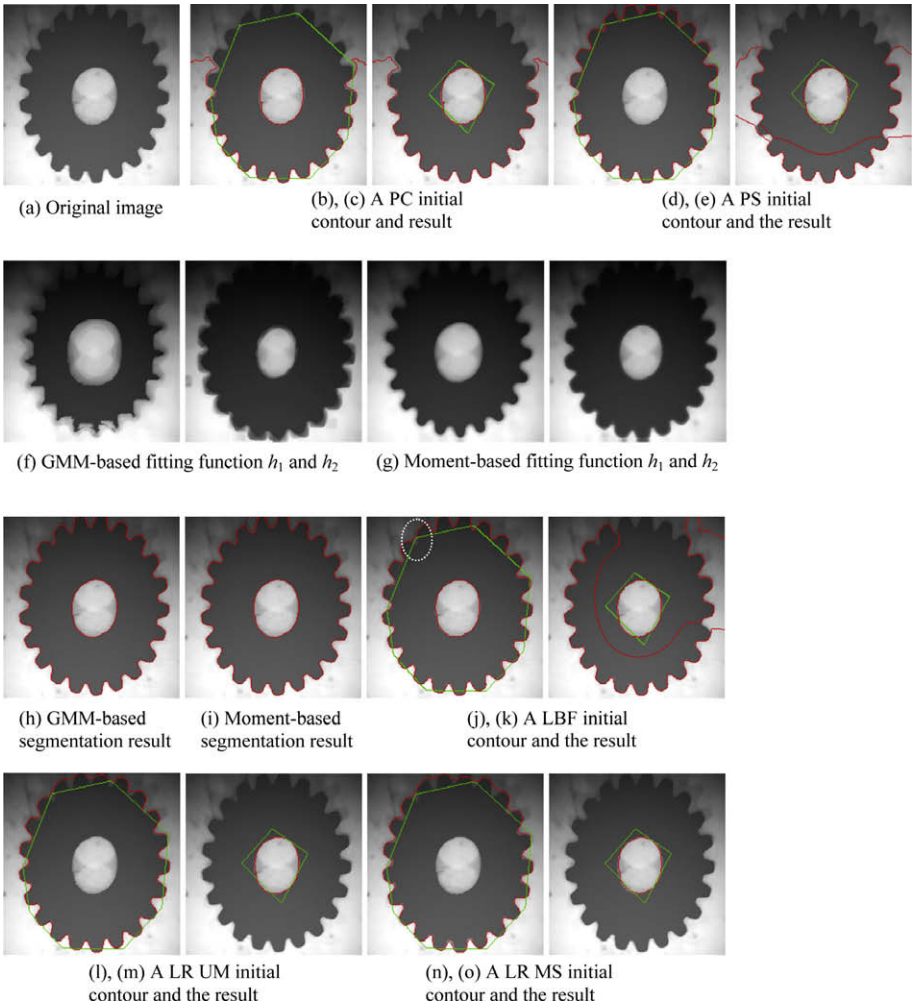

Fig. 5. Segmentation of a gear wheel image.

results with different initial contours. Fig. 3(f) and (g) show the GMM- and moment-based LDF fitting functions, h_1 and h_2. It can be seen that the points near boundaries have very different h_1 and h_2, which are almost the same for those points far away from boundaries. Figs. 3(j), 4(f) and 3(k), 4(g) are the LDF model segmentation results using the local GMM-based operator and the Hueckel operator, respectively. With simple objects in these images, both operators can generate accurate results. Fig. 3(h–j) show the local GMM-based segmentation results at different time steps, which demonstrate the emergence of new contours from the initial constant level set function. Similar results can also be obtained using the Hueckel operator. Figs. 3(l–m) and 4(h–i) are the LBF model segmentation results with different initial contours. The LBF model extracted different object boundaries with different initial contours, even with the same parameter settings. In practice, the LBF model initial contour has to be carefully selected for a successful segmentation. Figs. 3(n–o), 4(j–k) and 3(p–q), 4(l–m) show the extracted contours by the LR UM and MS energies, respectively, which significantly improves the performance of the original global energies. For example, the reformulated localized CV PC energy, i.e., the LR UM energy, obtains much better results than the global one.

Figs. 5(a) and 6(a) are five real images with complex object shapes or multiple objects placed in inhomogeneous and noisy background. Fig. 5(a) shows a wheel shape with multiple gears, and the objective is to extract both the inner and outer wheel boundaries. The wheel is locally darker than the background, though the bottom gear is brighter than the top background. The difficulty lies in the inhomogeneous and noisy background. There are multiple local energy minima in the background, e.g. the background dark blocks surrounded by brighter regions. As shown in Fig. 5(b–e), the global PC and PS models cannot accurately extract the complete wheel shape. Once more, the PS model shows better performance by successfully extracting the outer contour when the initial contour is close to the real boundary in Fig. 5(d). Fig. 5(f) and (g) show the GMM- and moment-based LDF fitting functions h_1 and h_2. Again, only the points close to boundary have a large difference of h_1 and h_2. The segmentation results based on the local GMM operator (Fig. 5(h)) and the Hueckel operator (Fig. 5(i)) are accurate and close to each other. With the initial contour in Fig. 5(j), the LBF model can extract most of the wheel boundary except two gears at the top left, as shown in the white dashed circle. With other initial contours (Fig. 5(k)), the LBF model cannot extract the wheel boundary correctly. Similar to the LBF model, with both initial contours, the LR UM (Fig. 5(l–m)) and MS (Fig. 5(n–o)) models cannot accurately extract both the inner and outer contours.

Fig. 6(a) show experiments on multiple objects segmentation. The global models are not included here due to inaccurate results (the PC model) or high computational cost (the PS model). Like Figs. 3–5, the LR UM and MS energies generate similar results, thus we present their "best" results here based on visual observations, which are all presented as the LR results. The LDF model using the outcomes of both the local GMM-based and the Hueckel operators obtained satisfactory results for all four images, as shown in

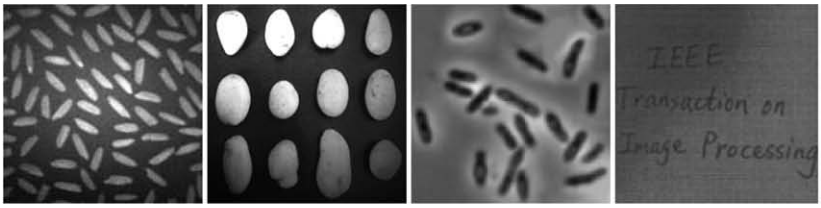

(a) Original images with rice, potatoes, bacteria, and handwriting words

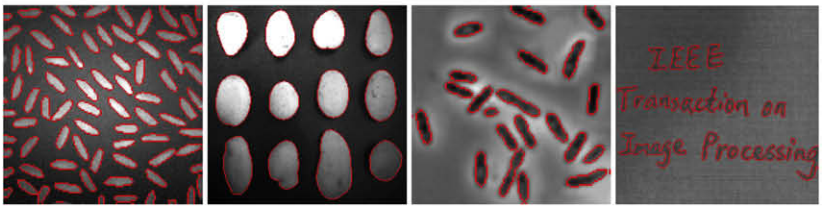

(b) GMM-based LDF segmentation results

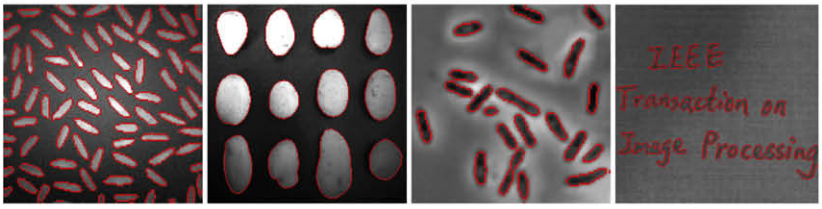

(c) Moment-based LDF segmentation results

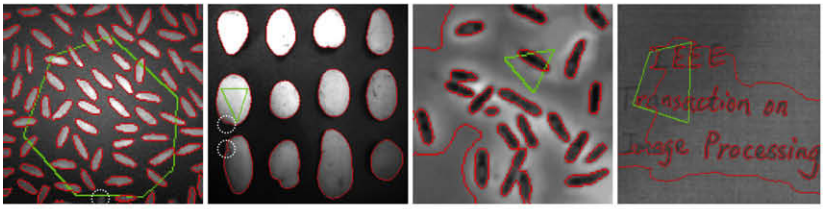

(d) LBF initial contours and segmentation results

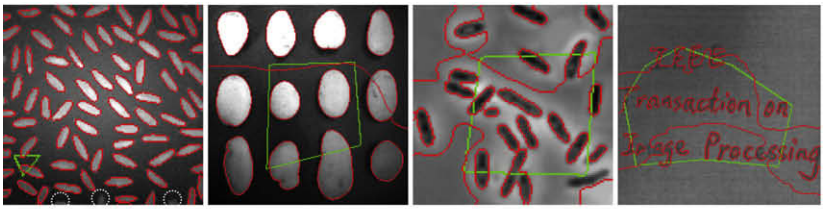

(e) LBF initial contours and segmentation results

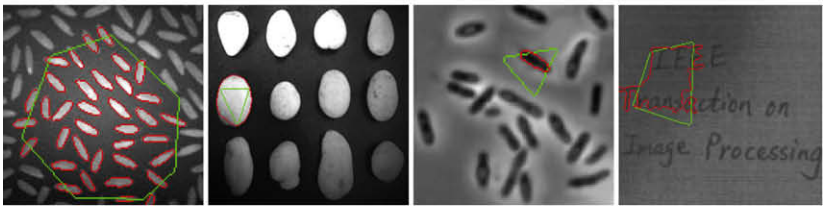

(f) LR initial contours and segmentation results

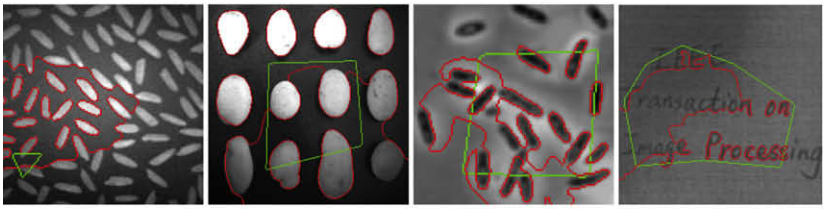

(g) LR initial contours and segmentation results

Fig. 6. Segmentation of images with rice, potatoes, bacteria, and handwriting words.

Fig. 6(b–c). For these complex segmentation problems, the LBF model has difficulty to accurately extract object boundaries. For example, the bottom rice grains in Fig. 6(d–e) and the two leftmost potatoes of the second and third rows in Fig. 6(d) have imprecise

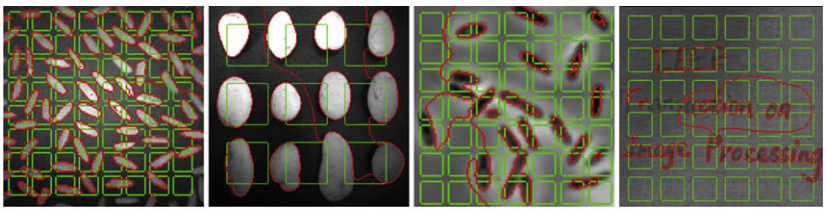

(h) LR initial contours and segmentation results

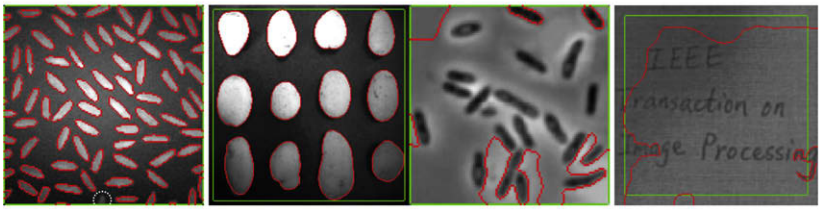

(i) LR initial contours and segmentation results

Fig. 6 (*continued*)

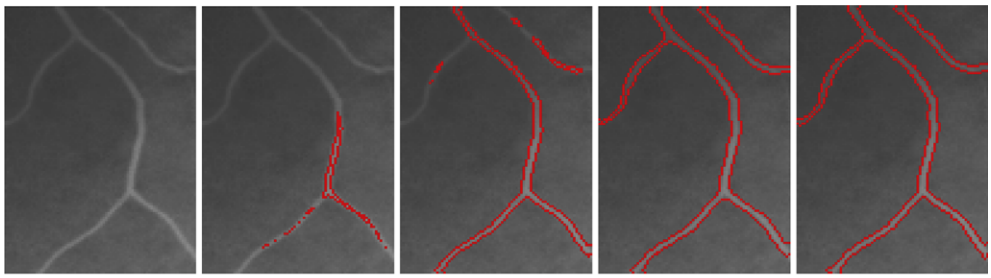

(a) Original image

(b), (c), (d) GMM-based segmentation results at 15, 60, and 250 iterations

(e) Moment-based segmentation result

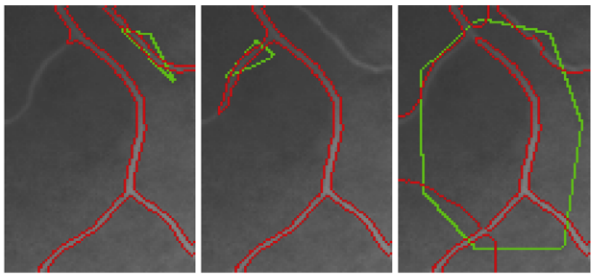

(f), (g), (h) LBF initial contours and segmentation results

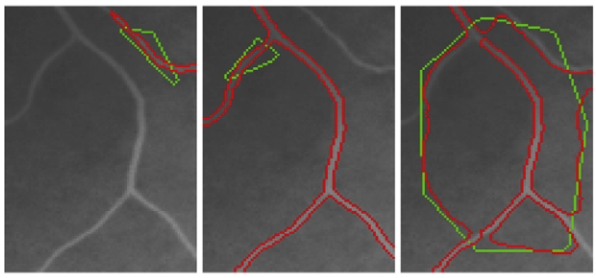

(i), (j), (k) LR initial contours and segmentation results

Fig. 7. Segmentation of an X-ray vessel image.

segmentation results, as shown in the white dashed circles. In addition, the LBF model is quite sensitive to the initial contours, as shown in Fig. 6(d–e). For the images of bacteria and handwriting words, the LBF model failed to extract the boundaries due to the complex object shapes and severe intensity inhomogeneity. With the poor contour initialization in Fig. 6(f–g), the LR models extract only a part of the object boundaries. To further test the LR model sensitivity on initial contours, we conduct two more experiments with multiple small initial contours (Fig. 6(h)) and one big initial contour (Fig. 6(i)) to enclose most objects. These initial contours significantly improve the segmentation results. For example, the LR model now can extract almost the perfect boundaries in the rice

and potato images in Fig. 6(i), except a minor rice grain at the bottom (see the white dashed circle). Though, similar to the LBF model, the LR model cannot handle the challenging cases of the bacterial and words images even with very good initial contours. The interested readers are referred to [18] for a more detailed discussion on the initialization sensitivity of the LR model.

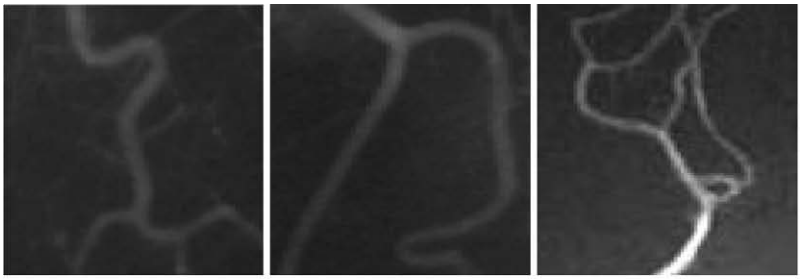

(a) Original X-ray vessel images

(b) GMM-based LDF segmentation results

(c) Moment-based LDF segmentation results

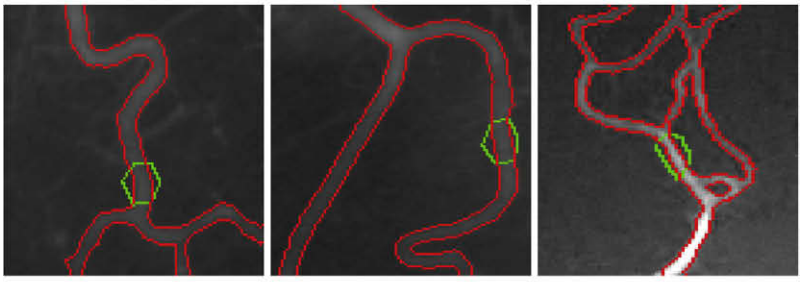

(d) LBF initial contours and segmentation results

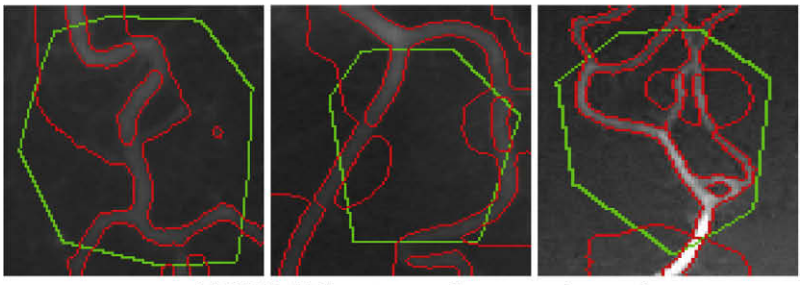

(e) LBF initial contours and segmentation results

Fig. 8. Segmentation of X-ray vessel images.

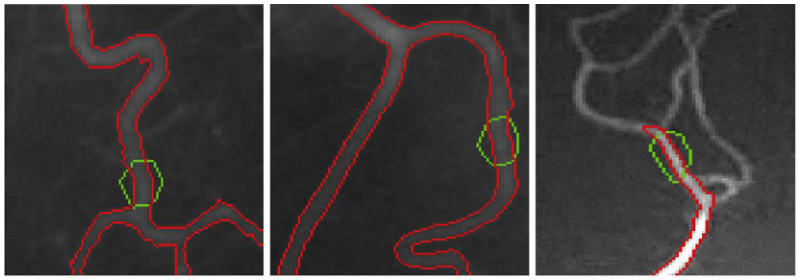

(f) LR initial contours and segmentation results

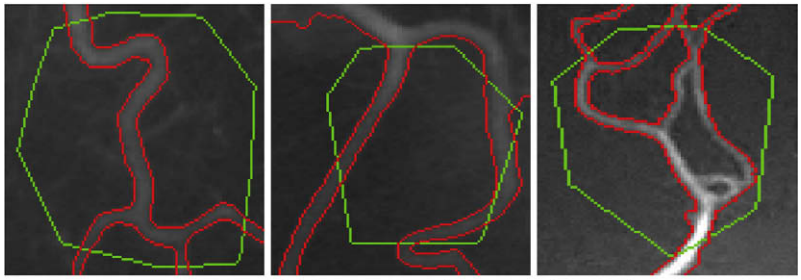

(g) LR initial contours and segmentation results

Fig. 8 (*continued*)

Figs. 7(a) and 8(a) are four X-ray vessel images with complex shapes of multiple branches (the first two images in Fig. 8(a) are from [19]). The goal is to extract the vessels from rather noisy and inhomogeneous background. The proposed LDF model successfully extracted the vessels from all the images, using both the local GMM-based operator and the Hueckel operator. The LBF model can extract the vessels in Fig. 8(d) with carefully selected initial contours. With other initial contours (Fig. 8(e)), it failed to extract the vessel boundaries. In addition, the LBF model cannot correctly extract all the vessel branches in Fig. 7(f–h) due to the very thin vessel branches at the left and right. It was able to extract either the left or the right branch when the initial contour was placed on it. The LR model obtains similar results as the LBF model in Fig. 7(i–k), i.e., only a part of the vessel boundary is extracted with all three initialization. With the initial contours in Fig. 8(f), the LR model correctly extracts the vessels in the left two images, but fails on the right one with severer noise and inhomogeneity. In Fig. 8(g), the LR model extracts the complete vessel shape in the left image, and most vessel boundaries in the right two images. In summary, like most existing active contours, the LBF model and the LR model are sensitive to the initial contour location, as shown in the experiments.

The three examples of Fig. 8 are used to compare the CPU times between the LDF model and the LBF model, which were recorded on an Dell OptiPlex™ GX620 Desktop PC, with Pentium(R) D 3.4 GHz CPU, 3.5 GB RAM, and Matlab 7.8 on Windows XP. The time costs of Fig. 8(b–d and f)[3] are listed in Table 1, from which it can be seen the GMM-based LDF model is the slowest (except the LR model) due to the iterative EM algorithm and the moment-based LDF model is the fastest. The time costs of the GMM- and moment-based operators to derive the LDF functions (h_1 and h_2) are also listed in Table 1 for a more detailed comparison. Note that our purpose here is to compare the relative speeds of these models under the same condition. Other fast algorithms [8,4,13] may be applied to these models for a reduced time cost. The GMM-based model and the moment-based model generally obtain rather close results for most images. Practically, we suggest the moment-based model for a much faster computation. As mentioned earlier, we do not suggest that one is superior to the other according to accuracy and robustness.

Table 1
CPU time (in second) comparison of Fig. 8.

		Left image	Middle image	Right image
Image size		110 × 110	131 × 103	78 × 103
GMM-based LDF model Fig. 8(b)	h_1 and h_2 estimation	9.00	10.12	5.91
	Total	10.76	17.00	8.33
Moment-based LDF model Fig. 8(c)	h_1 and h_2 estimation	0.14	0.14	0.11
	Total	4.81	8.94	1.77
LBF model Fig. 8(d)		5.80	11.09	2.03
LR model Fig. 8(f)		61.73	191.28	–

5. Summary

This paper presents a local distribution fitting model which integrates neighborhood-based intensity information into an edge-based implicit active contour for object boundary extraction. Our model incorporates traditional intensity distribution fitting and edge detection methods into a recent active contour (the LBF model), which preserves the good properties of both models and alleviates their difficulties, i.e., local intensity distribution fitting methods are good at edge detection, and the active contour always provides closed contours. This combination provides more accurate and robust segmentation than the LBF model. In the proposed LDF model, a localized GMM and Hueckel edge model are used to characterize the intensity distribution in the neighborhood of each image point. Specifically, only two local image features (i.e., two local means) are incorporated in the LDF model, which are sufficient to segment a large class of piecewise smooth images. With the pre-calculated LDF functions, our model does not require the user selection of the initial contour, which essentially alleviates the initialization sensi-

[3] Different from the LDF and the LBF models, the LR model is implemented with the narrowband level set method (http://www.shawnlankton.com/2008/04/active-contour-matlab-code-demo/), whose time costs are also listed in Table 1 as a general reference for interested readers.

tivity problem of most existing active contours. In addition, the LDF functions are calculated offline, which is more computationally efficient than the LBF model and many other local energy-based models. Experimental results on synthetic, natural and medical images show the improved performance of the LDF model over the global PC and PS models, and the LBF and LR models in inhomogeneous and noisy images. For future works, we will investigate the techniques to extend the LDF model to color or texture applications for real-world images [24,10].

Acknowledgments

The authors thank Chenyang Xu for the suggestions on algorithm development and presentation, Chunming Li and Shawn Lankton for sharing the code of the LBF model [19] and local region-based approach [18], and for their guidance on program parameter settings. The authors also thank the reviewers for valuable comments to improve this paper.

References

[1] L. Ambrosio, V.M. Tortorelli, Approximation of functionals depending on jumps by elliptic functionals via Γ-convergence, Communications on Pure and Applied Mathematics 43 (1990) 999–1036.
[2] L. Ambrosio, V.M. Tortorelli, On the approximation of free discontinuity problems, Bollettino Della Unione Matematica Italiana 7 (6-B) (1992) 105–123.
[3] K. Blekas, A. Likas, N.P. Galatsanos, I.E. Lagaris, A spatially constrained mixture model for image segmentation, IEEE Transactions on Neural Networks 16 (2) (2005) 494–498.
[4] X. Bresson, S. Esedoglu, P. Vandergheynst, J. Thiran, S. Osher, Fast global minimization of the active contour/snake model, Journal of Mathematical Imaging and Vision 28 (2) (2007) 151–167.
[5] T. Brox, D. Cremers, On the statistical interpretation of the piecewise smooth Mumford–Shah functional, in: Proceedings, International Conference on Scale Space Methods and Variational Methods in Computer Vision, 2007, pp. 203–213.
[6] V. Caselles, R. Kimmel, G. Sapiro, Geodesic active contours, International Journal of Computer Vision 22 (1) (1997) 61–79.
[7] A. Chakraborty, J.S. Duncan, Game-theoretic integration for image segmentation, IEEE Transactions on Pattern Analysis and Machine Intelligence 21 (1) (1999) 12–30.
[8] T.F. Chan, S. Esedoglu, M. Nikolova, Algorithms for finding global minimizers of image segmentation and denoising models, SIAM Journal on Applied Mathematics 66 (5) (2006) 1632–1648.
[9] T.F. Chan, L.A. Vese, Active contour without edges, IEEE Transactions on Image Processing 10 (2) (2001) 266–277.
[10] S. Chen, N.A. Sochen, Y.Y. Zeevi, Integrated active contours for texture segmentation, IEEE Transactions on Image Processing 15 (6) (2006) 1633–1646.
[11] D. Cremers, M. Rousson, R. Deriche, A review of statistical approaches to level set segmentation: integrating color, texture, motion and shape, International Journal of Computer Vision 72 (2) (2007) 195–215.
[12] A. Dempster, N. Laird, D. Rubin, Maximum likelihood from incomplete data via the EM algorithm, Journal of the Royal Statistical Society – Series B 39 (1) (1977) 1–38.
[13] T. Goldstein, X. Bresson, S. Osher, Geometric Applications of the Split Bregman Method: Segmentation and Surface Reconstruction, UCLA CAM Report [09–06], July 2009.
[14] J. Gomes, O. Faugeras, Reconciling distance functions and level sets, Journal of Visual Communication and Image Representation 11 (2) (2000) 209–223.
[15] L. Grady, C. Alvino, The piecewise smooth Mumford–Shah functional on an arbitrary graph, IEEE Transactions on Image Processing, in press.
[16] L. He, Z. Peng, B. Everding, X. Wang, C.Y. Han, K.L. Weiss, W.G. Wee, A comparative study of deformable contour methods on medical image segmentation, Image and Vision Computing 26 (2) (2008) 141–163.
[17] M. Hueckel, An operator which locates edges in digitized pictures, Journal of the ACM 18 (1) (1971) 113–125.
[18] S. Lankton, A. Tannenbaum, Localizing region-based active contours, IEEE Transactions on Image Processing 17 (11) (2008) 2029–2039.
[19] C. Li, C. Kao, J. Gore, Z. Ding, Minimization of region-scalable fitting energy for image segmentation, IEEE Transactions on Image Processing 17 (10) (2008) 1940–1949.
[20] C. Li, C. Xu, C. Gui, M.D. Fox, Level set evolution without re-initialization: a new variational formulation, in: Proceedings, IEEE Conference on Computer Vision and Pattern Recognition, 2005, pp. 430–436.
[21] C. Li, C. Xu, C. Gui, M.D. Fox, Distance regularized level set evolution and its application to image segmentation, IEEE Transactions on Image Processing, in press.
[22] E.P. Lyvers, O.R. Mitchell, M.L. Akey, A.P. Reeves, Subpixel measurements using a moment-based edge operator, IEEE Transactions on Pattern Analysis and Machine Intelligence 11 (12) (1989) 1293–1309.
[23] R. Malladi, J. Sethian, B. Vemuri, Shape modeling with front propagation, IEEE Transactions on Pattern Analysis and Machine Intelligence 17 (2) (1995) 158–171.
[24] U. Markus, P. Thomas, T. Werner, D. Cremers, B. Horst, TVSeg – interactive total variation based image segmentation, in: Proceedings, British Machine Vision Conference, 2008.
[25] G.J. McLachlan, D. Peel, Finite Mixture Models, Wiley, 2000.
[26] B. Mory, R. Ardon, Jean-Philippe Thiran, Variational segmentation using fuzzy region competition and local non-parametric probability density functions, in: Proceedings, IEEE International Conference on Computer Vision, 2007.
[27] D. Mumford, J. Shah, Optimal approximations by piecewise smooth functions and associated variational problems, Communications on Pure and Applied Mathematics 42 (5) (1989) 577–685.
[28] H. Permuter, J. Francos, I. Jermyn, A study of Gaussian mixture models of color and texture features for image classification and segmentation, Pattern Recognition 39 (4) (2006) 695–706.
[29] J. Piovano, M. Rousson, T. Papadopoulo, Efficient segmentation of piecewise smooth images, in: Proceedings, International Conference on Scale Space Methods and Variational Methods in Computer Vision, 2007, pp. 709–720.
[30] T. Pock, D. Cremers, H. Bischof, A. Chambolle, An algorithm for minimizing the Mumford–Shah functional, in: Proceedings, International Conference on Computer Vision, 2009.
[31] G. Sfikas, C. Nikou, N. Galatsanos, Edge preserving spatially varying mixtures for image segmentation, in: Proceedings, IEEE Conference on Computer Vision and Pattern Recognition, 2008.
[32] K. Sum, P. Cheung, Vessel extraction under non-uniform illumination: a level set approach, IEEE Transactions on Biomedical Engineering 55 (1) (2008) 358–360.
[33] M. Sussman, P. Smereka, S. Osher, A level set approach for computing solutions to incompressible two-phase flow, Journal of Computational Physics 114 (1) (1994) 146–159.
[34] A. Tsai, A. Yezzi, A.S. Willsky, Curve evolution implementation of the Mumford–Shah functional for image segmentation, denoising, interpolation, and magnification, IEEE Transactions on Image Processing 10 (8) (2001) 1169–1186.
[35] L.A. Vese, T.F. Chan, A multiphase level set framework for image segmentation using the Mumford and Shah model, International Journal of Computer Vision 50 (3) (2002) 217–293.
[36] X. Wang, L. He, W.G. Wee, Deformable contour method: a constrained optimization approach, International Journal of Computer Vision 59 (1) (2004) 87–108.
[37] M. Weber, A. Blake, R. Cipolla, Sparse finite elements for geodesic contours with level-sets, in: Proceedings, European Conference on Computer Vision, 2004, pp. 391–404.
[38] L. Xu, M. Jordan, On convergence properties of the EM algorithm for Gaussian mixtures, Neural Computation 8 (1) (1996) 129–151.
[39] S. Zhu, A. Yuille, Region competition: unifying snakes, region growing, and Bayes/MDL for multiband image segmentation, IEEE Transactions on Pattern Analysis and Machine Intelligence 18 (9) (1996) 884–900.